Article

The Transcriptome and Metabolome Reveal the Potential Mechanism of Lodging Resistance in Intergeneric Hybrids between *Brassica napus* and *Capsella bursa-pastoris*

Libin Zhang [1,2,†], Liyun Miao [1,3,†], Jianjie He [1], Huaixin Li [1] and Maoteng Li [1,*]

[1] College of Life Science and Technology, Huazhong University of Science and Technology, Wuhan 430074, China; libinzhang@hust.edu.cn (L.Z.); miaoliyun428@sxtcm.edu.cn (L.M.); jianjie_he@hust.edu.cn (J.H.); huaixin_lll@hust.edu.cn (H.L.)

[2] Hubei Bioinformatics & Molecular Imaging Key Laboratory, Department of Bioinformatics and Systems Biology, College of Life Science and Technology, Huazhong University of Science and Technology, Wuhan 430074, China

[3] College of Basic Medical Sciences, Shanxi University of Traditional Chinese Medicine, Jinzhong 030619, China

* Correspondence: limaoteng426@hust.edu.cn

† These authors have contributed equally to this work.

Abstract: Lodging is one of the main reasons for the reduction in seed yield and is the limitation of mechanized harvesting in *B. napus*. The dissection of the regulatory mechanism of lodging resistance is an important goal in *B. napus*. In this study, the lodging resistant *B. napus* line, YG689, derived from the hybridization between *B. napus* cv. Zhongyou 821 (ZY821) and *Capsella bursa-pastoris*, was used to dissect the regulation mechanism of hard stem formation by integrating anatomical structure, transcriptome and metabolome analyses. It was shown that the lignocellulose content of YG689 is higher than that of ZY821, and some differentially expressed genes (DEGs) involved in the lignocellulose synthesis pathway were revealed by transcriptome analyses. Meanwhile, GC–TOF–MS and UPLC–QTOF–MS identified 40, 54, and 31 differential metabolites in the bolting stage, first flower stage, and the final flower stage. The differential accumulation of these metabolites might be associated with the lignocellulose biosynthesis in *B. napus*. Finally, some important genes that regulate the metabolic pathway of lignocellulose biosynthesis, such as *BnaA02g18920D*, *BnaA10g15590D*, *BnaC05g48040D*, and NewGene_216 were identified in *B. napus* through the combination of transcriptomics and metabolomics data. The present results explored the potential regulatory mechanism of lignocellulose biosynthesis, which provided a new clue for the breeding of *B. napus* with lodging resistance in the future.

Keywords: *Brassica napus*; lignocellulose; transcriptome; differentially expressed genes; metabolome

1. Introduction

B. napus is one of the most important oil crops in the world, and the stem tissue is an advantageous energy material for the development of biodiesel. Crop lodging was mainly induced because of stem fall caused by strong winds and other factors, as well as root fall caused by poor root anchorage strength [1]. Stem strength, i.e., the bending and/or breaking strength of the culm, is important for stem lodging resistance [2]. The stem strength of crops is primarily determined by plant architecture (morphological traits and anatomical structure) [3]. In particular, the anatomical structure is a consequence of plant growth and development at the cellular level, such as cell division, cell growth, and cell spatial arrangement, and it is closely related to environmental factors. For example, the stem with a large diameter and a thick cell wall could increase the bending strength and lodging resistance of wheat, barley, and rice stems [2,4,5]. Plant height is considered to be an important morphological feature affecting crop lodging, but it is not the main factor determining crop lodging [6,7]. Lignocellulose is a major component of the

mechanical strength of crop stems [8], and its content is related to the lodging resistance of crops [3,5,9]. Lignin and cellulose determine the mechanical strength of the stem [10], while the accumulation of starch could also increase the flexural strength and hardness of the stem [11]. Peng et al. [12] and Berry et al. [1] found that the increase in lignin and hemicellulose content could enhance the stalk strength and lodging resistance of wheat.

Metabolomics provides a powerful way to study the metabolic phenotype of *Brassica* species [13–16]. Tan et al. [13] identified the dynamic metabolic changes from both seeds and silique walls that occur during oil accumulation by using gas chromatography coupled with mass spectrometry (GC–MS) and demonstrated that the oil content was independent of leaf photosynthesis and phloem transport during oil accumulation, but it required the metabolic influx from the silique wall. Kortesniemi et al. [16] investigated NMR metabolomics of ripened and developing oilseed rape (*B. napus*) and turnip rape (*B. rapa*) and found differences in the major lipids and the minor metabolites between the two species. High-throughput sequencing is one of the important tools used to study important agronomic traits and gene expression regulation in *B. napus* [17–21]. For example, Li et al. [18] identified 71 candidate genes with stem lodging-related traits through the genome-wide association study (GWAS) method, and constructed a gene co-expression network based on transcriptome sequencing, which revealed the genetic basis of stem lodging traits in *B. napus*. Kawakatsu et al. [21] reported the phenotypic and transcriptomic landscape of 61 rice (*Oryza sativa*) accessions with highly diverse below-ground traits grown in an upland field, which provided a useful resource for understanding the genomic and transcriptomic bases of phenotypic variation under upland field conditions. The metabolomics analysis is the quantitative detection of all metabolites and their biochemical states in specific organisms or tissues. Moreover, high-throughput sequencing has been combined with metabolomics data to explore the complex regulatory metabolism networks [22–29]. For example, Guo et al. [29] characterized the acclimation of maize (*Zea mays* B73) to drought and cold stresses using physiological measurements and comparative transcriptomics combined with metabolomics during the stress treatments and recovery stages, which presented a model showing that the plant response to the combined stress is multi-faceted and revealed an ABA-dependent maize acclimation mechanism to the stress combination. However, there is a lack of a systematic investigation of the lignocellulose-related gene expression networks through the combination of different omics technologies.

Interspecific and intergeneric hybridization are widely used to create the new germplasm with valuable characteristics. Zhongyou 821 (ZY821) is a winter rapeseed variety with a high yield that is multi resistant with a wide adaptability, which was cultivated in China for many years [30]. Park [31] found that the content of erucic acid in the rapeseed oil of *C. bursa-pastoris* was significantly lower than that of other cruciferous plants. Moreover, *C. bursa-pastoris* displayed high resistance to black spot disease and *Sclerotinia sclerotiorum* [32,33] and could endure cold, salt, and drought stress [34], which was probably related to its lignified or wooden stems. Furthermore, the hybridizations between *B. napus* (2n = 38; female) and *C. bursa-pastoris* (male, 2n = 32) were performed in the fields by hand emasculation and pollination [33]. The stably inherited hybrids with the expected chromosome number and normal meiosis behaviors were screened. Coincidently, a hard stem material, YG689, was identified in its offspring population. YG689 was reported to contain high lignin content, a certain resistance to *Sclerotinia sclerotiorum,* and the obvious characteristics of its *C. bursa-pastoris* origin, such as wooden stems [33]. In addition, Shen et al. [35] obtained one doubled haploid (DH) population obtained from a cross between Y689 and *B. napus* var. Westar, and the QTL for the plant height (PH), branch initiation height (BIH), stem diameter (SD), and flowering time (FT) were obtained.

Although some studies had been carried out for the YG689, the molecular regulatory mechanism and metabolic pathway of lodging resistance still remains elusive in YG689. In the present study, the regulatory mechanism for the stem lodging resistance of YG689 was studied by combining the anatomical structure, comparative transcriptomic and metabolomic analyses. The present results shed light on the molecular regulatory

pathways in lignocellulose biosynthesis, which provides a new clue for the breeding of *B. napus* with lodging resistance in the future.

2. Results

2.1. The Anatomical Structure and Lignocellulose Analysis of ZY821 and YG689

The stems of ZY821 and YG689 in the early flowering and maturation stages were used for the morphological and anatomical analyses. As shown in Figure 1C, the stem strength and dry weight of YG689 were significantly higher than that of ZY821. These results indicate that the YG689 had stronger stem lodging resistance than that of ZY821. To explore the difference in stem anatomical structure, the stems of YG689 and ZY821 were evenly divided into five sections from bottom to top (Figure 1B). It was revealed that the lateral distribution of lignin in YG689 was obviously wider than that of ZY821 (Figure 2). The stem anatomical structures between YG689 and ZY821 at the maturation stage were also compared, and similar results were obtained (Figure S1).
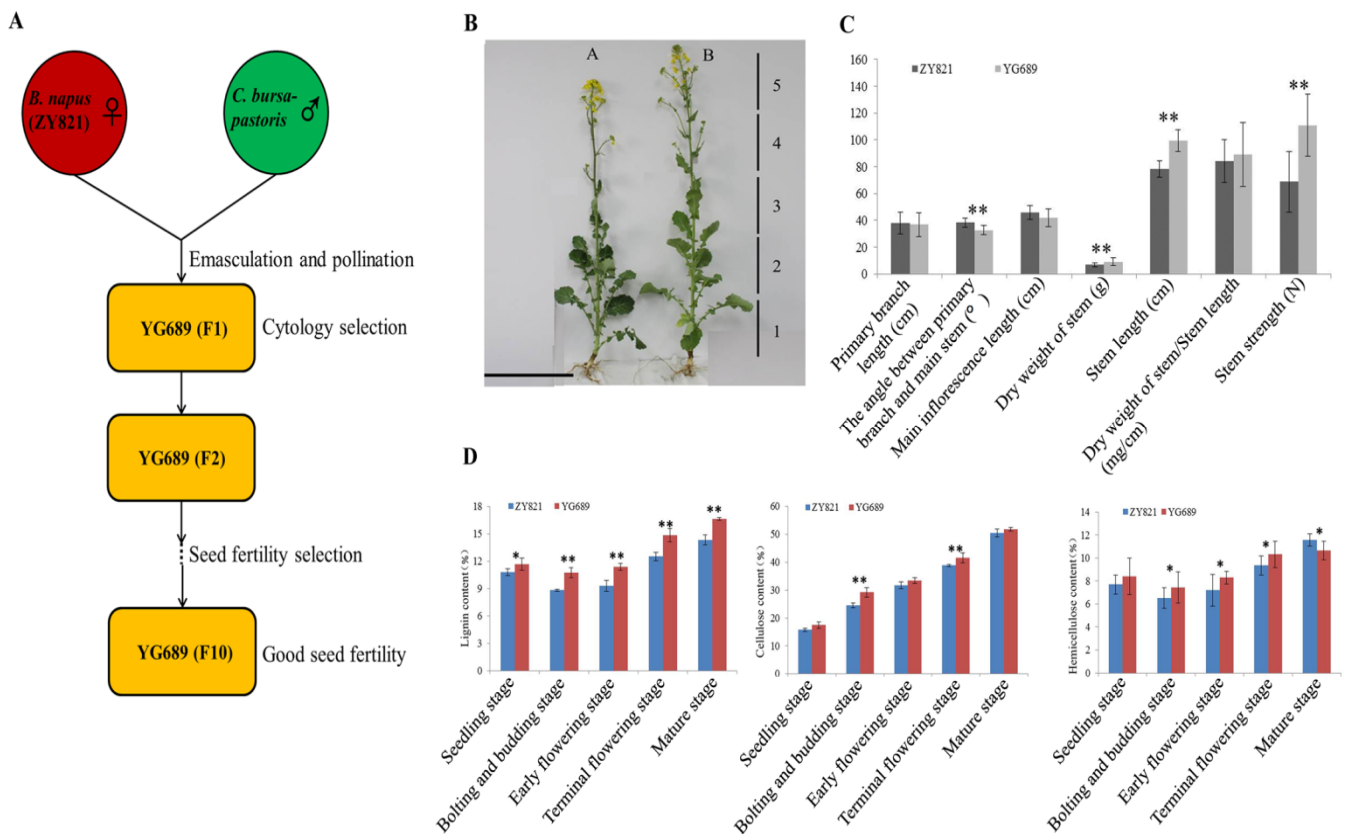
Figure 1. (**A**) The sketch map of YG689 generation from the hybridization of ZY821 and *C. bursa-pastoris*. (**B**) The morphology of ZY821 (Left) and YG689 (Right) at initial flowering stage. Bar = 50 cm. (**C**) The morphology analysis of ZY821 and YG689 at the mature stage (fifteen biological replicates). (**D**) Comparison of stem lignocellulose (lignin, cellulose, and hemicellulose) content of ZY821 and YG689 at five development stages (three biological replicates). * Significant at $p < 0.05$; ** significant at $p < 0.01$.

Figure 2. Transverse stem sections of ZY821 and YG689 at initial flowering stage. Stained red characteristics represent the distribution of lignin. The plant is divided into five parts from the base to the top, in turn, and labeled 1, 2, 3, 4, and 5. Bar = 2 mm.
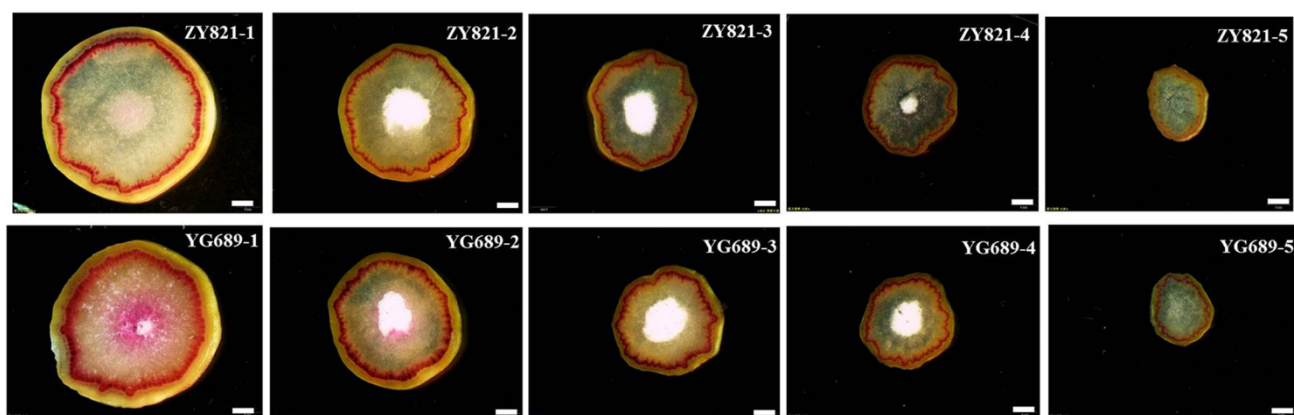
To further analyze the difference in the lignocellulose components in stems between YG689 and ZY821, the content of lignocellulose in the YG689 and ZY821 stems at the seedling, bolting and budding, early flowering, terminal flowering, and maturation stages were measured. It was revealed that the lignin content of YG689 was significantly higher than that of ZY821 at all stages ($p < 0.05$), and the cellulose content of YG689 was significantly higher than that of ZY821 at the bolting and budding stage and the terminal flowering stage ($p < 0.01$) (Figure 1D). The content of hemicellulose was also significantly higher in YG689 than that of ZY821 ($p < 0.05$) except at the seedling stage. The lignin monomers in YG689 and ZY821 stems at different developmental stages were further analyzed by using the GC–MS. It was found that the G monolignol was the main monomer, and the content in YG689 was higher than that of ZY821 at the seedling stage (Table S1). Further analyses showed that the S monolignol also existed, but the content of the S monolignol was lower than that of the G monolignol in both YG689 and ZY821 (Table S1).

2.2. Transcriptome Analysis of YG689 and ZY821

The transcriptome of YG689 and ZY821 for the stem at the initial flowering stage were analyzed by RNA-Seq technology, where 99,472,340 (SRA number: SRX1522099) and 134,015,130 (SRA number: SRX1142564) clean reads, after removing adaptor sequences and low-quality reads, were generated, respectively. It was revealed that 88.35% (87,884,725) of YG689 and 90.60% (121,415,423) of ZY821 clean reads were mapped to the *B. napus* genome, among which 79.08% (78,663,759) and 61.44% (82,335,196) of clean reads were uniquely mapped to the *B. napus* genome. The trinity program was then applied for the de novo assembly of the clean reads, and 2697 novel genes were identified by comparing the assembled transcripts with the genome annotation information of *B. napus*. The genes were then annotated to the COG, NR, Swiss-Prot, GO, and KEGG databases (Table S2). Among these novel genes, 339 were annotated by COG (12.57%), 1509 were annotated by GO (55.95%), 418 were annotated by KEGG (15.50%), 1348 (49.98%) were annotated with Swiss-Prot, and 2284 (84.69%) were annotated with NR.

To reveal the global differential gene expression profiles between YG689 and ZY821, the DEGs, by setting the gene expression level of ZY821 as a control, were analyzed, and the up- or down-regulated genes in YG689 were observed. In total, 8644 DEGs (3818 up-regulated and 4826 down-regulated genes) were identified (Figure 3A). Thirteen DEGs were randomly selected for RT-qPCR validation. The majority of the expression trends of selected DEGs were consistent with the RNA-seq results (Figure 3B), which indicated the reliability of transcriptome sequencing results. The DEGs between YG689 and ZY821 were further annotated with Gene Ontology terms, which could be classified into three categories and 51 subcategories (Figure S2). For example, the "cellular process", "metabolic process",

and "single-organism process" in the biological process were enriched in most of the DEGs. The DEGs were also analyzed by the Cytoscape Enrichment Map based on the GO annotation, and a total of 4873 DEGs were enriched in the biological process category (Figure S3). The overlapping terms between up-regulated and down-regulated genes were "metabolic process", "response to stimulus", "biological regulation", "developmental process", "localization" and "cellular process". Importantly, we found that the up-regulated DEGs in YG689 were mainly assigned to the "rhythmic process", "cellular component biogenesis", and "signaling" terms, which suggested the activities of the cell metabolism and signal transductions were much more active in YG689 than in ZY821. To better understand the biological functions of DEGs between YG689 and ZY821, the DEGs were further assigned for the KEGG analysis (Supplementary Dataset S1 with the listed top-20 pathways) and some important pathways associated with lignocellulose synthesis were found, including "arginine and proline metabolism", "cysteine and methionine metabolism", "carotenoid biosynthesis", and "glutathione metabolism". Moreover, the DEGs involved in these KEGG pathways were localized on the *B. napus* genome (Figure 4). Among them, 30 DEGs were found to be significantly associated with lignocellulose synthesis (Table S3). For example, GH9B17, TPS1, UGE4, and GAUT13 were up-regulated in the "starch and sucrose metabolism" pathway in YG689. (Figure 5). Twelve DEGs related to the lignocellulose synthesis were randomly selected for further expression analyses in the stem of YG689, ZY821, and TN070 (another *B. napus* line with a soft stem) in bolting, early flowering, and final flowering stages. It was shown that nine DEGs were significantly up-regulated in the early-flowering stage of YG689, and the up-regulation of *BnaA09g42650* persisted to the final flowering stage and reached the highest value (Figure 3C). For example, *BnaA09g42650* is homologous to PRX17 in *Arabidopsis*, and the transcription factor AGL15 participates in the transition of vegetative growth to reproductive growth, as well as the formation of lignification tissues, by directly regulating PRX17. Therefore, we speculated that the hybridization between *C. bursa-pastoris* and ZY821 leads to the differential expression of lignin synthesis-related genes, which induced the stem traits of YG689.

Further analyses revealed that 624 DEGs could not be compared to the *B. napus* reference genome, 108 of which could be compared to the *C. bursa-pastoris* genome. Twenty-three DEGs have more than 40% of the homology rate and six DEGs have more than 80% of the homology rate. The 23 DEGs were subjected to KEGG analysis and five new genes (New-Gene_6090, NewGene_3494, NewGene_1078, NewGene_2975, and NewGene_3483) were annotated. NewGene_6090 is homologous to Carubv10019973m (Vacuolar ATP synthase subunit A, VHA-A) of *C. bursa-pastoris* and participated in the oxidative phosphorylation pathway; NewGene_3494 is homologous to Carubv10003976m (RNA polymerase II large subunit, NRPB1) of *C. bursa-pastoris* and participates in the purine or pyrimidine metabolism pathway; NewGene_1078 is homologous to Carubv10011493m (2-oxoglutarate, 2OG) of *C. bursa-pastoris* and is involved in cysteine and methionine metabolism; New-Gene_2975 is homologous to Carubv10001560m (syntaxin of plants 132, SYP132) of *C. bursa-pastoris* and is involved in SNARE interactions in the vesicular transport pathway; and NewGene_3483 is homologous to Carubv10008883m (beta glucosidase 40, BGLU40) of *C. bursa-pastoris* and is involved in starch and sucrose metabolism or phenylpropane biosynthesis. Notably, another 516 DEGs could not be compared to the *B. napus* genome and the *C. bursa-pastoris* genome, which indicates that these DEGs might be novel genes that derived from the chromosome exchange between *B. napus* and *C. bursa-pastoris*.
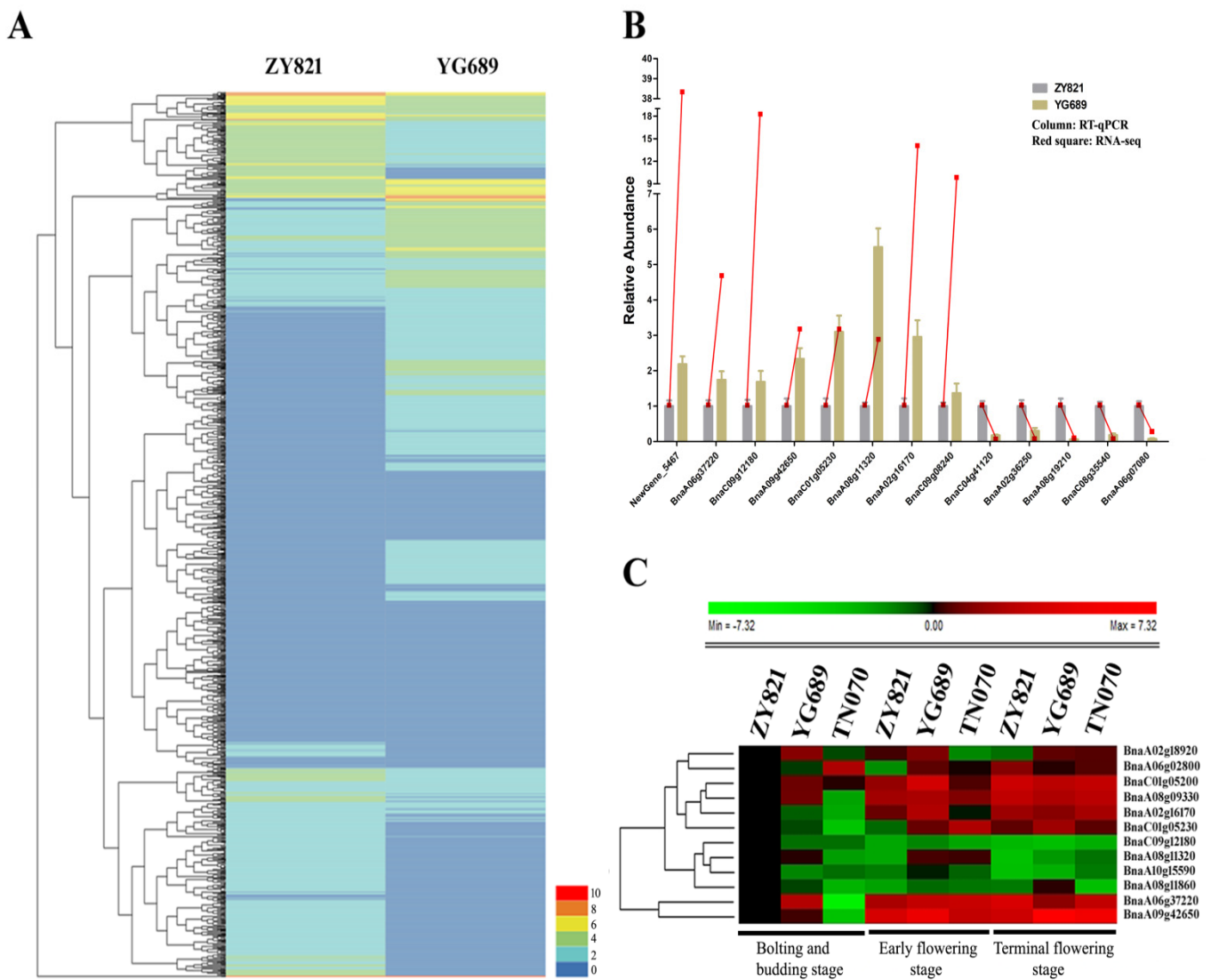
Figure 3. (**A**) Heatmap analysis of differentially expressed genes between YG689 and ZY821. RPKM (reads per kb per million reads) was used to calculate gene expression level. The color key (0, 2, 4, 6, 8, 10) represents FPKM normalized log(10) transformed counts. Red represents high expression and blue represents low expression. Each row represents a gene. (**B**) Validation of differentially expressed genes by RT-qPCR. Thirteen DEGs were randomly chosen for RT-qPCR validation using ZY821 transcript expression levels as the control. The relative expression levels of each gene are expressed as the fold change between ZY821 and YG689. The *B. napus* ACT 7 actin gene is used as an internal control. Histogram indicated the relative expression level between ZY821 and YG689 from RT-qPCR results and red square indicated the relative expression level between ZY821 and YG689 from RNA-seq. (**C**) Heatmap analysis of lignocellulose-related DEGs among ZY821, YG689, and TN070. The color key represents relative expression levels normalized log 2-transformed counts. Red represents high expression and green represents low expression. Each row represents a gene (*n* = 3).
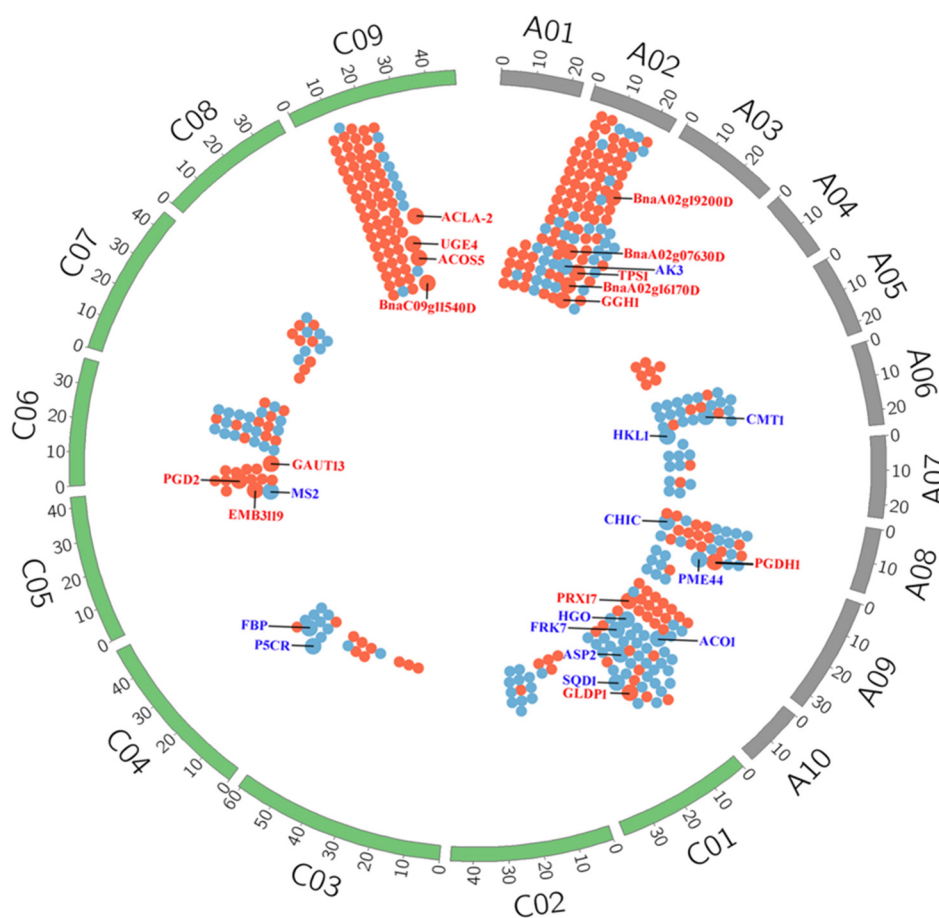
Figure 4. The distribution of the DEGs involved in KEGG pathways on *B. napus* genome. A01-A10 indicates 10 chromosomes of A genome in *B. napus*; C01-C09 indicates 9 chromosomes of C genome in *B. napus*. Red dots indicate up-regulated genes and blue dots indicate down-regulated genes. Large dots indicate 30 DEGs closely related to lignocellulose synthesis.

2.3. Metabolome Analysis of Stem of YG689 and ZY821

To reveal the differential metabolites in the stem of YG689 and ZY821, the metabolomics of the stems of YG689 and ZY821 in the bolting, early flowering, and terminal flowering stages were also analyzed by using the GC–TOF–MS and UPLC–QTOF–MS techniques. A total of 449 peaks were obtained by the GC–TOF–MS analysis, and the PCA score map of the metabolic spectrum showed that all the YG689 and ZY821 samples were in the 95% confidence interval (Figure S4). Twenty differential metabolites between YG689 and ZY821 at the bolting stage were identified (Table S4), and the content of 19 metabolites in YG689 were lower than that of ZY821, which included saccharides (sucrose, L-threose, ribulose-5-phosphate, D- galactose, raffinose, and tagatose), amino acids and derivatives (L-valine, β-alanine and threo-beta-hyrdoxyaspartate) and other products of plant metabolism in *B. napus*. Twenty-six differential metabolites were identified in the early flowering stage (Table S4), and the content of eight metabolites in YG689 is higher than that of ZY821, which included maleamate, elaidic acid, succinic acid, malonic acid, L-valine, 5, 6-dihydrouracil, erythrose and mannitol. Seven differential metabolites between YG689 and ZY821 at the final flowering stage were obtained (Table S4), and four metabolites in YG689 were higher than of ZY821, including glutaconic acid, inosine, nornicotine, and leucrose.

Figure 5. Analysis of metabolic pathways of the lignocellulose-related DEGs. The red arrows represent the up-regulated gene, and blue arrows represent the down-regulated gene.

The UPLC–QTOF–MS was also used to detect the differential metabolites between YG689 and ZY821, and 25, 36, and 39 differential metabolites were observed in the bolting, early flowering, and final flowering stages, respectively (Table S5). In the bolting stage, the content of proline was increased in YG689, while 5-L-glutamyl-L-alanine, deoxyadenosine, and kaempferol were decreased in YG689 (Table S5). In the early flowering stage, the content of L-threonate, aconitate, and (S)-2-hydroxyglutarate increased in YG689, while cytidine, guanosine, and cytidine 2′, 3′-cyclic phosphate decreased in YG689 (Table S5). In the final flowering stage, the content of beta-D-fructose 6-phosphate, D-gluconate and L-isoleucine increased in YG689, while the content of N,N′-Diacetylchitobiose, alpha-linolenic acid, L-leucine and succinate decreased in YG689 (Table S5).

Furthermore, the metabolites identified by GC–TOF–MS and UPLC–QTOF–MS were integrated together, and 40, 54, and 31 differential metabolites between YG689 and ZY821 in the bolting, initial flowering, and final flowering stages were identified, respectively. These differential metabolites were involved in nine important metabolic pathways (Table S6), including glycolysis; the TCA cycle; the pentose phosphate pathway; fructose and mannose metabolism; galactose metabolism; phenylalanine, tyrosine, and tryptophan synthesis; starch and sucrose metabolism; glycine, serine, and threonine metabolism; and cysteine and methionine metabolism. For example, cis-aconitate and succinate were common differential metabolites in three developmental stages and were involved in TCA cycle pathways. Finally, the related metabolic pathway of lignocellulose synthesis was constructed by integrating DEGs and differential metabolites in the stem of YG689 and ZY821 (Figure 6), which consisted of 14 distinct metabolites and four important DEGs that might regulate the lignocellulose synthesis.
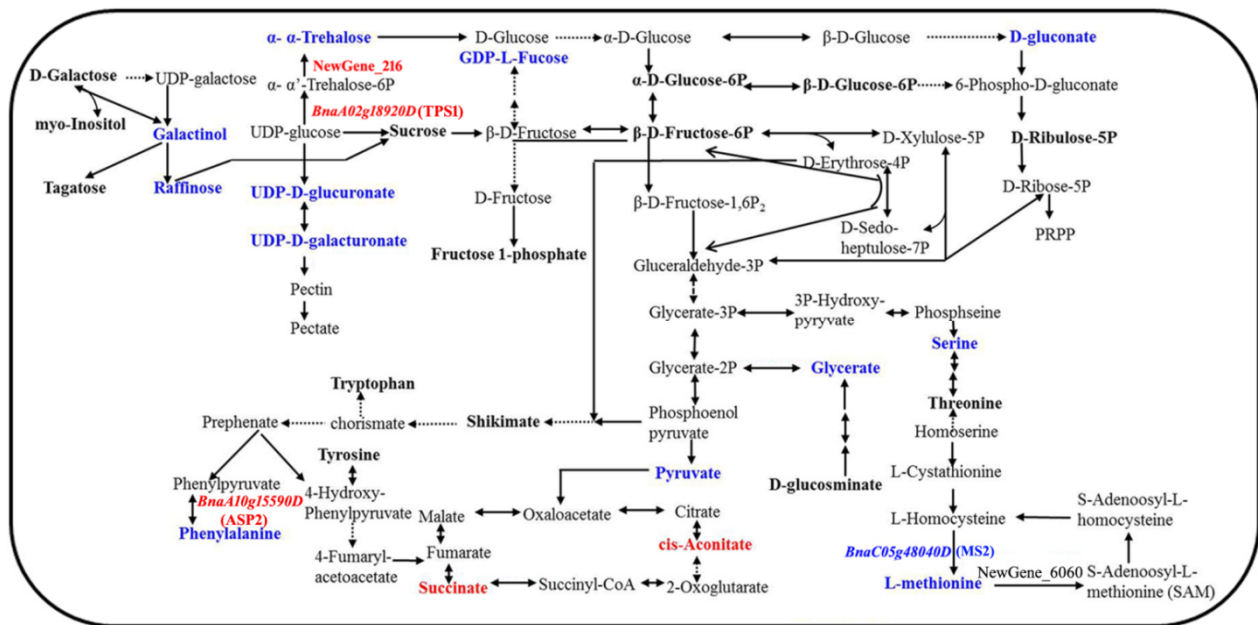
Figure 6. Metabolic pathway of lignocellulose by integrating DEGs, differentially accumulated metabolites between ZY821 and YG689. Red marks indicate up-regulated genes or up-accumulated metabolites in the pathway of lignocellulose synthesis. Blue marks indicate down-regulated genes or down-accumulated metabolites in the pathway of lignocellulose synthesis. NewGene_216 and NewGene_6060 are predicted new genes for *B. napus* by transcriptome analysis.

2.4. The Validation of DEGs Regulating the Metabolic Pathway of Lignocellulose Synthesis

The level of secondary metabolites is associated with gene expression, protein modification, and the response to environmental changes in the growth and development process of plant. A total of four DEGs (*BnaA02g18920D*, *BnaA10g15590D*, NewGene_216, and *BnaC05g48040D*) were identified to be the key enzyme genes and were involved in the regulation of lignocellulose synthesis (Figure 6). The RT-qPCR validation results were shown in Figure S5. For example, the expression of *BnaA02g18920D* (TPS1) increased, which may facilitate the production of Trehalose 6-phosphate (T6P) and the development of a hard stem in YG689. In addition, *BnaA10g15590D* is homologous with the ASP2 gene of *Arabidopsis* and participates in phenylalanine biosynthesis. *BnaA10g15590D* was up-regulated in YG689, which may stimulate the level of phenylalanine biosynthesis in the metabolic pathway of lignocellulose. Nevertheless, *BnaC05g48040D* (MS2) was down-regulated in YG689, which indicates the decrease in the phenylalanine and L-methionine levels in the metabolic pathway of lignocellulose. Meanwhile, some new genes that were expressed in YG689 derived from the *C. bursa-pastoris* genome were also identified. For example, NewGene_216 was predicted to be trehalose-phosphate synthase 7, which catalyzes UDP glucose to form trehalose-6-phosphate and participates in the synthesis of trehalose. Interestingly, although the expression of NewGene_216 increased, the content of trehalose decreased in YG689. We guessed that the content of trehalose was transformed by other pathways. Therefore, we speculated that these DEGs might affect the lignocellulose synthesis in the stem tissues of YG689, thus affecting the stem hardness in *B. napus*.

3. Discussion

Distant hybridization is an important way to create new germplasm resources [36]. For example, Liu et al. [37] transferred the clubroot-resistance genes from clubroot-resistant Chinese cabbages to *B. napus* by distant hybridization combined with embryo rescue. Gong et al. [38] obtained the hybrids with powdery mildew (PM) resistance through hybridization between the *B. napus* cultivar 'Zhongshuang11' and the PM-resistant *B. carinata*. Lodging is one of the main reasons that influences mechanized harvesting, which

results in yield reduction [39]. Long et al. [40] reported that *Oryza longistaminata* has a strong stem and a high biomass productivity, and 12, 11, and 3 QTLs for the stem diameter (SD), stem length (SL), and breaking strength (BS), respectively, were obtained in the mapping population that was obtained between line 93–11 and *O. longistaminata*. In the previous studies, a germplasm of YG689 with high fertility and lodging resistance was obtained in the offspring that were derived from *B. napus* and *C. bursa-pastoris*, and further analyses revealed that YG689 had a high content of lignin [33]. Intensive research on the lodging resistance mechanism of YG689 is helpful to cultivate the new *B. napus* lines with lodging resistance characteristics.

Transcriptomic analyses have been widely used to find the candidate genes or study the regulatory mechanisms of important agronomic traits. For example, four candidate genes that regulate the lignin content were identified by the integration of GWAS and transcriptome sequencing, which provides insight into the genetic control of lodging and lignin in *B. napus* [17]. The unique QTLs for stem lodging-related traits (plant height, branch initiation height, and stem diameter) were found by Shen et al. [35] in *B. napus*, and some genes (including ESK1 and CESA6) involved in lodging resistance have been identified [18]. Li et al. [41] reported that the CESA9 conserved-site mutation could affect its association with the CESA complexes and cause the low-DP (degree of polymerization) cellulose synthesis, which significantly enhanced plant lodging resistance and biomass enzymatic saccharification in rice. In the present study, some DEGs that were closely related to lignocellulose synthesis were identified between ZY821 and YG689, and most of these DEGs were located in the main QTLs regions reported by Shen et al. [35]. Meanwhile, 624 DEGs could not be mapped to the *B. napus* genome, and 108 DEGs could be mapped to the *C. bursa-pastoris* genome. Some genes that were associated with the lignocellulose biosynthesis were included. For example, *BnaA09g42650* is homologous with PRX17 from *Arabidopsis*. PRX17 encodes a cell wall-localized class III peroxidase and is involved in lignified tissue formation. The transcription factor AGL15 (agamous-like15) directly regulates PRX 17 and participates in the transition from vegetative growth to reproductive growth and the formation of lignified tissue in *A. thaliana* [42]. Interestingly, 516 of 624 DEGs could be neither mapped to the *B. napus* nor mapped to the *C. bursa-pastoris* genome, which indicates that these new genes might derive from the genome recombination between *B. napus* and *C. bursa-pastoris.* Coincidentally, Zhang et al. [43] identified 37 HE (homologous exchange) events in the progeny of a nascent allotetraploid (AADD) from two diploid progenitors of hexaploid bread wheat. The obtained HEs are highly enriched within gene bodies, giving rise to novel recombinant genes. Furthermore, the generation of chimeric genes was detected in the HEs of the allopolyploid *Brassica*, rice, *Arabidopsis suecica*, banana, and peanut [43], which provides a mechanism for the generation of new genes and new proteins in nascent allopolyploids.

Recently, the integration analysis of the transcriptome and metabolome has been applied to reveal the regulatory pathways of specific agronomic traits in *B. napus* [44–49]. For example, Jia et al. [44] performed the metabolomic and transcriptomic analyses of the yellow-flowered rapeseed cultivar ZS11 and the white-flowered inbred line WP, and it was shown that the white petal color in WP flowers is primarily due to decreased lutein and zeaxanthin contents, and BnNCED4b might play a key role in white petal formation. Tan et al. [45] investigated the gene expression profiles and metabolite content by the integration analysis of the transcriptome and metabolome in the seeds of *B. napus*. It was revealed that the expression of major carbohydrate metabolism-regulating genes was significantly correlated with carbohydrate content during seed maturation. In the present study, we integrated the DEGs and differential metabolites to construct a specific pathway of the lignocellulose metabolism in YG689. Notably, a total of 14 distinct metabolites and four DEGs were found to be involved in the regulation of lignocellulose synthesis. For example, the content of cis-aconitate and succinate was higher in the stem of YG689 than in ZY821 in three developmental stages. Importantly, cis-aconitate and succinate are involved in the TCA cycle pathway. Therefore, we speculate that the more active tricarboxylic

acid cycle pathway promotes lignin synthesis in YG689 in comparison with ZY821. TPS1 is a gene coding for an enzyme that catalyzes the production of Trehalose 6-phosphate (T6P). It was reported that TPS1 is mainly expressed in axillary buds and the subtending vasculature, as well as in the leaf and stem vasculature [50]. A recent study showed that TPS1 is associated with the traits of plant height, peduncle length, and biomass in wheat [51]. Moreover, it was shown that the loss of TPS1 in *A. thaliana* impaired high-temperature-mediated hypocotyl growth [52]. Our study found that TPS1 was highly expressed in the stem tissue and up-regulated in YG689 compared with ZY821. Further integration analyses of the transcriptome and metabolome revealed that TPS1 was involved in the regulation of lignocellulose synthesis, which broadens our understanding of key genes regulating important agronomic traits of crops. In addition, as the most abundant pectic glycan, Homogalacturonan (HG) functions as a cell wall structural and signaling molecule essential for plant growth, development, and responses to pathogens [53]. GAUT13 was reported to de novo synthesize HG in the absence of exogenous HG acceptors [53]. In this study, GAUT13 was found to be up-regulated in YG689 (Table S3), which suggests the functional significance of GAUT13 in the lignocellulose synthesis of *B. napus*. However, the exact mechanism of GAUT13 regulating the lignocellulose synthesis in *B. napus* needs to be further explored in the future. Lignocellulose is a major component of the mechanical strength of the crop stem tissue and is related to the lodging resistance of crops. The present results are not only useful for understanding the potential regulatory mechanism of lignocellulose biosynthesis, but they also suggest a novel strategy for breeding new varieties with lodging resistance traits, ultimately increasing rapeseed yield in the future.

4. Materials and Methods

4.1. Plant Materials

The seeds of YG689, ZY821, *C. bursa-pastoris,* and TN070 (the *B. napus* line with a soft stem) are provided by Professor Zaiyun Li of Huazhong Agricultural University, China. YG689 was selected from the successive cytological and fertility selection in the offspring derived from the hybridization between *B. napus* var. ZY821 and *C. bursa-pastoris* (Figure 1A). The materials were planted in the experimental field of Huazhong Agricultural University from 2013 to 2016. The seeds were generally sown in late September of the year and the plants and seeds were collected in early May of following year. The row spacing was 40 cm and the plant spacing was 20 cm.

4.2. Anatomical Structure and Lignocellulose Content Analysis of YG689 and ZY821

Stem samples of YG689 and ZY821 at the early flowering and mature stages with three replicates were evenly divided into five segments from the base to the top (Figure 1B). The middle part of the segment was taken for anatomic observation. Some of the transected materials were stained with 1% resorcinol (dissolved in 95% alcohol) for 2 min, then stained with concentrated hydrochloric acid for 1 min, and finally were observed and photographed by the stereomicroscope (Olympus MVX10, Japan). Meanwhile, the stem samples of YG689 and ZY821 at the seedling, bolting and budding, early flowering, final flowering, and maturation stages with three replicates were collected for the lignocellulose total content analysis. The seedling, bolting and budding, early flowering, final flowering, and maturation stages were 105, 142, 160, 178, and 215 days after sowing, respectively. The different developmental stages of stems were firstly blanched at 105°C and dried at 60 °C, and 5 mg of YG689 and ZY821 stalk powder were put into 10 mL test tubes for lignocellulose total content measurements, respectively. The acetyl bromide method was used to extract and detect lignin [54], and the content was calculated according to the Bouguer–Lambert–Beer law method [55]. The lignin monomer was prepared as previously described [56], and its contents were determined by GC–MS analysis. The cellulose and hemicellulose were extracted and detected according to the previous literature [57].

Fifteen whole plant materials of YG689 and ZY821 were randomly selected, and the stem length was measured after removing the roots. Furthermore, the 20-cm stems were

cut from the stem base and were put on the stem strength tester (YYD-1) to measure the stem strength index. Stem fiber components were measured by near-infrared reflectance spectroscopy (NIRS) using NIR (FOSS, NIRS 5000) with WinISI software, according to previous reports [17]. Five random plants for YG689 and ZY821 were selected and their stems at 20 cm above the cotyledon scar were intercepted, dried, and ground into powder for measuring the fiber components. The phenotype values for acid detergent lignin (ADL), acid detergent fiber (ADF), and neutral detergent fiber (NDF) were speculated from NIRS spectra using NIRS calibrations for these traits, as described by Wei et al. [17].

4.3. RNA Extraction and Transcriptome Sequencing

Total RNAs were extracted from the stems of YG689 and ZY821 by the TriZol method (Invitrogen, Carlsbad, CA, USA), and the mRNAs were isolated from total RNA using Dynabeads oligo (dT) (Invitrogen). First- and second-strand cDNA were synthesized using Superscript II reverse transcriptase and random hexamer primers. Double-stranded cDNA was fragmented by nebulization and used to generate RNA-seq libraries, as previously described [58]. Three biological replicates of the cDNA libraries were sequenced using the Illumina Hiseq 2000 platform. The mRNA expression levels in YG689 and ZY821 were verified by using RT-qPCR. One microgram of total RNA was reverse-transcribed using SuperScript III reverse transcriptase and oligo (dT)18, according to the manufacturer's instructions. The RT-qPCR reaction system was performed by using the TOYOBO SYBR® R Green Realtime PCR Master Mix (code No. QPK-201) kit. RNA-seq data showed that the mRNA level of actin in ZY821 and YG689, or in each growth stage (the bolting stage, early flowering stage, and terminal flowering stage) was stable. Therefore, actin was set as the reference gene in RT-qPCR experiments. The primers for mRNA RT-qPCR are listed in Table S7. The relative expression levels of these genes were measured by the $2^{-\Delta\Delta Ct}$ method using RT-qPCR.

4.4. Differentially Genes Expression and Function Enrichment Analysis

The differentially expressed genes (DEGs) between YG689 and ZY821 were identified using the expression levels of ZY821 transcripts as the control and were tested with the software package DESeq (version 1.12.3) [59] with a false discovery rate (FDR) of < 0.01 and a normalized fold change of $\geq$2. The GO enrichment analysis applied a hypergeometric test to find significantly enriched GO terms in DEGs comparing the genome background [60], where the calculating formula was the same as previously described [61], and the GO terms, with an adjusted *p*-value of 0.05, were defined as significantly enriched GO terms in DEGs. The enriched GO categories were visualized using the Cytoscape plug-in Enrichment Map (http://www.cytoscape.org/ (19/08/2021)). DEGs which could not be mapped to the *B. napus* reference genome [62] were aligned to the *C. bursa-pastoris* reference genome [63] to predict the origin and function of them.

4.5. Metabolome Analysis of YG689 and ZY821

Six biological replicates of each stem sample (0.05 g per sample) of YG689 and ZY821 in the bolting, early flowering, and terminal flowering stages were collected. A total of 36 stem samples were extracted for the GC–TOF–MS analysis, as previously described [64]. An Agilent 7890 GC system equipped with a Pegasus 4D TOFMS (LECO, St. Joseph, MI, USA) was used for the GC–TOF–MS analysis. Metabolite quantification was performed using a multiple reaction monitoring (MRM) method, as described [65]. Statistical significance was defined at $p < 0.05$, with highly significant values at $p < 0.01$. The VIP (variable importance in the projection) value (threshold > 1) of the first principal component of OPLS-DA model and the *p* value of the *t*-test (threshold 0.05) are used to identify the differentially expressed metabolites.

Supplementary Materials: The following are available online at https://www.mdpi.com/article/10.3390/ijms23094481/s1.

References

1. Berry, P.M.; Spink, J.H.; Gay, A.P.; Craigon, J. A comparison of root and stem lodging risks among winter wheat cultivars. *J. Agric. Sci.* **2003**, *141*, 191–202. [CrossRef]
2. Zuber, U.; Winzeler, H.; Messmer, M.M.; Keller, M.; Stampet, P. Morphological traits associated with lodging resistance of spring wheat (*Triticumae stivum* L.). *J. Agron. Crop Sci* **1999**, *182*, 17–24. [CrossRef]
3. Zhang, Y.; Liu, P.; Zhang, X.; Zheng, Q.; Chen, M.; Ge, F.; Li, Z.; Sun, W.; Guan, Z.; Liang, T.; et al. Multi-Locus Genome-Wide Association Study Reveals the Genetic Architecture of Stalk Lodging Resistance-Related Traits in Maize. *Front. Plant Sci.* **2018**, *9*, 611. [CrossRef]
4. Kashiwagi, T.; Ishimaru, K. Identification and functional analysis of a locus for improvement of lodging resistance in rice. *Plant. Physiol.* **2004**, *134*, 676–683. [CrossRef]
5. Pinthus, M.J. Lodging in wheat, barley and oats: The phenomenon, its causes and preventative measures. *Adv. Agron.* **1973**, *25*, 210–263.
6. Ma, J.F.; Yamaji, N. Silicon uptake and accumulation in higher plants. *Trends Plant Sci.* **2006**, *11*, 392–397. [CrossRef]
7. Islam, M.S.; Peng, S.; Visperas, R.M.; Ereful, N.; Bhuiya, M.; Julfiquar, A.W. Lodging-related morphological traits of hybrid rice in a tropical irrigated ecosystem. *Field Crop Res.* **2007**, *101*, 240–248. [CrossRef]
8. Ma, Q.H.; Xu, Y.; Lin, Z.B.; He, P. Cloning of cDNA encoding COMT from wheat which is differentially expressed in lodging-sensitive and-resistant cultivars. *J. Exp. Bot.* **2002**, *53*, 2281–2282. [CrossRef]
9. Ookawa, T.; Inoue, K.; Matsuoka, M.; Ebitani, T.; Takarada, T.; Yamamoto, T.; Ueda, T.; Yokoyama, T.; Sugiyama, C.; Nakaba, S.; et al. Increased lodging resistance in long- culm, low-lignin gh2 rice for improved feed and bioenergy production. *Sci. Rep.* **2014**, *4*, 6567. [CrossRef]
10. Ookawa, T.; Ishihara, K. Varietal differences of physical characteristics of the culm related to lodging in paddy rice. *Jpn. J. Crop Sci.* **1992**, *61*, 419–425. [CrossRef]
11. Kashiwagi, T.; Madoka, Y.; Hirotsu, N.; Ishimaru, K. Locus prl5 improves lodging resistance of rice by delaying senescence and increasing carbohydrate reaccumulation. *Plant Physiol. Biochem.* **1992**, *44*, 152–157. [CrossRef] [PubMed]
12. Peng, D.; Chen, X.; Yin, Y.; Lu, K.; Yang, W.; Tang, Y.; Wang, Z. Lodging resistance of winter wheat (*Triticumae stivum* L.) lignin accumulation and its related enzymes activities due to the application of paclobutrazol or gibberellin acid. *Field Crop Res.* **2014**, *157*, 1–7. [CrossRef]
13. Tan, H.; Xie, Q.; Xiang, X.; Li, J.; Zheng, S.; Xu, X.; Guo, H.; Ye, W. Dynamic metabolic profiles and tissue specific source effects on the metabolome of developing seeds of *Brassica napus*. *PLoS ONE* **2015**, *10*, e0124794. [CrossRef]
14. Tan, H.; Xiang, X.; Tang, J.; Wang, X. Nutritional functions of the funiculus in *Brassica napus* seed maturation revealed by transcriptome and dynamic metabolite profile analyses. *Plant Mol. Biol.* **2016**, *92*, 539–553. [CrossRef] [PubMed]
15. Borisjuk, L.; Neuberger, T.; Schwender, J.; Heinzel, N.; Sunderhaus, S.; Fuchs, J.; Hay, J.O.; Tschiersch, H.; Braun, H.P.; Denolf, P.; et al. Seed architecture shapes embryo metabolism in oilseed rape. *Plant Cell.* **2013**, *25*, 1625–1640. [CrossRef] [PubMed]
16. Kortesniemi, M.; Vuorinen, A.L.; Sinkkonen, J.; Yang, B.; Rajala, A.; Kallio, H. NMR metabolomics of ripened and developing oilseed rape (*Brassica napus*) and turnip rape (*Brassica rapa*). *Food Chem.* **2015**, *172*, 63–70. [CrossRef] [PubMed]
17. Wei, L.; Jian, H.; Lu, K.; Yin, N.; Wang, J.; Duan, X.; Li, W.; Liu, L.; Xu, X.; Wang, R.; et al. Genetic and transcriptomic analyses of lignin- and lodging-related traits in *Brassica napus*. *Theor. Appl. Genet.* **2017**, *130*, 1961–1973. [CrossRef]
18. Li, H.; Cheng, X.; Zhang, L.; Hu, J.; Zhang, F.; Chen, B.; Xu, K.; Gao, G.; Li, H.; Li, L.; et al. An Integration of Genome-Wide Association Study and Gene Co-expression Network Analysis Identifies Candidate Genes of Stem Lodging-Related Traits in *Brassica napus*. *Front. Plant Sci.* **2018**, *9*, 796. [CrossRef]
19. Wei, C.; Zhu, L.; Wen, J.; Yi, B.; Ma, C.; Tu, J.; Shen, J.; Fu, T. Morphological, transcriptomics and biochemical characterization of new dwarf mutant of *Brassica napus*. *Plant Sci.* **2018**, *270*, 97–113. [CrossRef]
20. Miller, C.N.; Harper, A.L.; Trick, M.; Wellner, N.; Werner, P.; Waldron, K.W.; Bancroft, I. Dissecting the complex regulation of lodging resistance in *Brassica napus*. *Mol. Breed.* **2018**, *38*, 30. [CrossRef]

21. Kawakatsu, T.; Teramoto, S.; Takayasu, S.; Maruyama, N.; Nishijima, R.; Kitomi, Y.; Uga, Y. The transcriptomic landscapes of rice cultivars with diverse root system architectures grown in upland field conditions. *Plant J.* **2021**, *106*, 1177–1190. [CrossRef] [PubMed]

22. Dobrowolska, I.; Businge, E.; Abreu, I.N.; Moritz, T.; Egertsdotter, U. Metabolome and transcriptome profiling reveal new insights into somatic embryo germination in Norway spruce (*Picea abies*). *Tree Physiol.* **2017**, *37*, 1752–1766. [CrossRef] [PubMed]

23. Huang, H.; Yao, Q.; Xia, E.; Gao, L. Metabolomics and Transcriptomics Analyses Reveal Nitrogen Influences on the Accumulation of Flavonoids and Amino Acids in Young Shoots of Tea Plant (*Camellia sinensis* L.) Associated with Tea Flavor. *J. Agric. Food Chem.* **2018**, *66*, 9828–9838. [CrossRef] [PubMed]

24. Li, Y.; Wang, W.; Feng, Y.; Tu, M.; Wittich, P.E.; Bate, N.J.; Messing, J. Transcriptome and metabolome reveal distinct carbon allocation patterns during internode sugar accumulation in different sorghum genotypes. *Plant Biotechnol. J.* **2019**, *17*, 472–487. [CrossRef] [PubMed]

25. Reem, N.T.; Chen, H.Y.; Hur, M.; Zhao, X.; Wurtele, E.S.; Li, X.; Li, L.; Zabotina, O. Comprehensive transcriptome analyses correlated with untargeted metabolome reveal differentially expressed pathways in response to cell wall alterations. *Plant Mol. Biol.* **2018**, *96*, 509–529. [CrossRef]

26. Verhoeven, K.J.F.; Verbon, E.H.; van Gurp, T.P.; Oplaat, C.; Ferreira de Carvalho, J.; Morse, A.M.; Stahl, M.; Macel, M.; McIntyre, L.M. Intergenerational environmental effects: Functional signals in offspring transcriptomes and metabolomes after parental jasmonic acid treatment in apomictic dandelion. *New Phytol.* **2018**, *217*, 871–882. [CrossRef]

27. Kumar, R.; Gyawali, A.; Morrison, G.D.; Saski, C.A.; Robertson, D.J.; Cook, D.D.; Tharayil, N.; Schaefer, R.J.; Beissinger, T.M.; Sekhon, R.S. Genetic Architecture of Maize Rind Strength Revealed by the Analysis of Divergently Selected Populations. *Plant Cell Physiol.* **2021**, *62*, 1199–1214. [CrossRef]

28. Yu, M.; Wang, M.; Gyalpo, T.; Basang, Y. Stem lodging resistance in hulless barley: Transcriptome and metabolome analysis of lignin biosynthesis pathways in contrasting genotypes. *Genomics* **2021**, *113*, 935–943. [CrossRef]

29. Guo, Q.; Li, X.; Niu, L.; Jameson, P.E.; Zhou, W. Transcription-associated metabolomic adjustments in maize occur during combined drought and cold stress. *Plant Physiol.* **2021**, *186*, 677–695. [CrossRef]

30. Zhao, J.; Buchwaldt, L.; Rimmer, S.R.; Sharpe, A.; McGregor, L.; Bekkaoui, D.; Hegedus, D. Patterns of differential gene expression in *Brassica napus* cultivars infected with *Sclerotinia sclerotiorum*. *Mol Plant Pathol.* **2009**, *10*, 635–649. [CrossRef]

31. Park, R.J. The occurrence of mustard oil glucosides in *Lepidium hyssopifolium* Desv., L. bonariense (L.) and *Capsella bursa* pastoris (L.) Medic. *Aust. J. Chem.* **1967**, *20*, 799–2801. [CrossRef]

32. Sigareva, M.A.; Earle, E.D. Regeneration of plants from protoplasts of Capsella bursa-pastoris and somatic hybridization with rapid cycling *Brassica oleracea*. *Plant Cell Rep.* **1999**, *18*, 412–417. [CrossRef]

33. Chen, H.F.; Wang, H.; Li, Z.Y. Production and genetic analysis of partial hybrids in intertribal crosses between *Brassica* species (*B. rapa*, *B. napus*) and *Capsella bursa-pastoris*. *Plant Cell Rep.* **2007**, *26*, 1791–1800. [CrossRef] [PubMed]

34. Liu, S.; Wang, X.; Fan, Z.; Pang, Y.; Sun, X.; Wang, X.; Tanga, K. Molecular cloning and characterization of a novel cold-regulated gene from *Capsella bursa-pastoris*. *DNA Seq.* **2004**, *15*, 262–268. [CrossRef]

35. Shen, Y.; Xiang, Y.; Xu, E.; Ge, X.; Li, Z. Major Co-localized QTL for Plant Height, Branch Initiation Height, Stem Diameter, and Flowering Time in an Alien Introgression Derived *Brassica napus* DH Population. *Front. Plant Sci.* **2018**, *9*, 390. [CrossRef]

36. Chen, Z.J. Genetic and epigenetic mechanisms for gene expression and phenotypic variation in plant polyploids. *Ann. Rev. Plant Biol.* **2007**, *58*, 377–406. [CrossRef]

37. Liu, Y.; Xu, A.; Liang, F.; Yao, X.; Wang, Y.; Liu, X.; Zhang, Y.; Dalelhan, J.; Zhang, B.; Qin, M.; et al. Screening of clubroot-resistant varieties and transfer of clubroot resistance genes to *Brassica napus* using distant hybridization. *Breed Sci.* **2018**, *68*, 258–267. [CrossRef]

38. Gong, Q.; Dai, C.Y.; Zhang, X.H.; Wang, X.L.; Huang, Z.; Xu, A.X.; Dong, J.G.; Yu, C.Y. Towards breeding of rapeseed (*Brassica napus*) with alien cytoplasm and powdery mildew resistance from Ethiopian mustard (*Brassica carinata*). *Breed Sci.* **2020**, *70*, 387–395. [CrossRef]

39. Kendall, S.L.; Holmes, H.; White, C.A.; Clarke, S.M.; Berry, P.M. Quantifying lodging-induced yield losses in oilseed rape. *Field Crop Res.* **2017**, *211*, 106–113. [CrossRef]

40. Long, W.; Dan, D.; Yuan, Z.; Chen, Y.; Jin, J.; Yang, W.; Zhang, Z.; Li, N.; Li, S. Deciphering the Genetic Basis of Lodging Resistance in Wild Rice Oryza longistaminata. *Front. Plant Sci.* **2020**, *11*, 628. [CrossRef]

41. Li, F.; Xie, G.; Huang, J.; Zhang, R.; Li, Y.; Zhang, M.; Wang, Y.; Li, A.; Li, X.; Xia, T.; et al. OsCESA9 conserved-site mutation leads to largely enhanced plant lodging resistance and biomass enzymatic saccharification by reducing cellulose DP and crystallinity in rice. *Plant Biotechnol. J.* **2017**, *15*, 1093–1104. [CrossRef] [PubMed]

42. Cosio, C.; Ranocha, P.; Francoz, E.; Burlat, V.; Zheng, Y.; Perry, S.E.; Ripoll, J.J.; Yanofsky, M.; Dunand, C. The class III peroxidase PRX17 is a direct target of the MADS-box transcription factor AGAMOUS-LIKE15 (AGL15) and participates in lignified tissue formation. *New Phytol.* **2017**, *213*, 250–263. [CrossRef] [PubMed]

43. Zhang, Z.; Gou, X.; Xun, H.; Bian, Y.; Ma, X.; Li, J.; Li, N.; Gong, L.; Feldman, M.; Liu, B.; et al. Homoeologous exchanges occur through intragenic recombination generating novel transcripts and proteins in wheat and other polyploids. *Proc. Natl. Acad. Sci. USA* **2020**, *117*, 14561–14571. [CrossRef] [PubMed]

44. Jia, L.; Wang, J.; Wang, R.; Duan, M.; Qiao, C.; Chen, X.; Ma, G.; Zhou, X.; Zhu, M.; Jing, F.; et al. Comparative transcriptomic and metabolomic analyses of carotenoid biosynthesis reveal the basis of white petal color in *Brassica napus*. *Planta* **2021**, *253*, 8. [CrossRef]

45. Tan, H.; Zhang, J.; Qi, X.; Shi, X.; Zhou, J.; Wang, X.; Xiang, X. Correlation analysis of the transcriptome and metabolome reveals the regulatory network for lipid synthesis in developing *Brassica napus* embryos. *Plant Mol. Biol.* **2019**, *99*, 31–44. [CrossRef]

46. Wang, W.; Pang, J.; Zhang, F.; Sun, L.; Yang, L.; Zhao, Y.; Yang, Y.; Wang, Y.; Siddique, K.H.M. Integrated transcriptomics and metabolomics analysis to characterize alkali stress responses in canola (*Brassica napus* L.). *Plant Physiol. Biochem.* **2021**, *166*, 605–620. [CrossRef]

47. Courbet, G.; D'Oria, A.; Maillard, A.; Jing, L.; Pluchon, S.; Arkoun, M.; Pateyron, S.; Paysant Le Roux, C.; Diquélou, S.; Ourry, A.; et al. Comparative Omics Analysis of *Brassica napus* Roots Subjected to Six Individual Macronutrient Deprivations Reveals Deficiency-Specific Genes and Metabolomic Profiles. *Int. J. Mol. Sci.* **2021**, *22*, 1679. [CrossRef]

48. D'Oria, A.; Jing, L.; Arkoun, M.; Pluchon, S.; Pateyron, S.; Trouverie, J.; Etienne, P.; Diquélou, S.; Ourry, A. Transcriptomic, Metabolomic and Ionomic Analyses Reveal Early Modulation of Leaf Mineral Content in *Brassica napus* under Mild or Severe Drought. *Int. J. Mol. Sci.* **2022**, *23*, 781. [CrossRef]

49. Raza, A.; Su, W.; Hussain, M.A.; Mehmood, S.S.; Zhang, X.; Cheng, Y.; Zou, X.; Lv, Y. Integrated Analysis of Metabolome and Transcriptome Reveals Insights for Cold Tolerance in Rapeseed (*Brassica napus* L.). *Front. Plant Sci.* **2021**, *12*, 721681. [CrossRef]

50. Fichtner, F.; Barbier, F.F.; Annunziata, M.G.; Feil, R.; Olas, J.J.; Mueller-Roeber, B.; Stitt, M.; Beveridge, C.A.; Lunn, J.E. Regulation of shoot branching in arabidopsis by trehalose 6-phosphate. *New Phytol.* **2021**, *229*, 2135–2151. [CrossRef]

51. Lyra, D.H.; Griffiths, C.A.; Watson, A.; Joynson, R.; Molero, G.; Igna, A.A.; Hassani-Pak, K.; Reynolds, M.P.; Hall, A.; Paul, M.J. Gene-based mapping of trehalose biosynthetic pathway genes reveals association with source- and sink-related yield traits in a spring wheat panel. *Food Energy Secur.* **2021**, *10*, e292. [CrossRef]

52. Hwang, G.; Kim, S.; Cho, J.Y.; Paik, I.; Kim, J.I.; Oh, E. Trehalose-6-phosphate signaling regulates thermoresponsive hypocotyl growth in *Arabidopsis thaliana*. *EMBO Rep.* **2019**, *20*, e47828. [CrossRef] [PubMed]

53. Engle, K.A.; Amos, R.A.; Yang, J.Y.; Glushka, J.; Atmodjo, M.A.; Tan, L.; Huang, C.; Moremen, K.W.; Mohnen, D. Multiple Arabidopsis galacturonosyltransferases synthesize polymeric homogalacturonan by oligosaccharide acceptor-dependent or de novo synthesis. *Plant J.* **2021**, *109*, 1441–1456. [CrossRef] [PubMed]

54. Van, A.R.; Vanholme, R.; Storme, V.; Mortimer, J.C.; Dupree, P.; Boerjan, W. Lignin biosynthesis perturbations affect secondary cell wall composition and saccharification yield in *Arabidopsis thaliana*. *Biotechnol. Biofuels.* **2013**, *6*, 46.

55. Chang, X.F.; Chandra, R.; Berleth, T.; Beatson, R.P. Rapid, microscale, acetylbromide-based method for high-throughput determination of lignin content in Arabidopsis thaliana. *J. Agric. Food Chem.* **2008**, *56*, 6825–6834. [CrossRef]

56. Chen, F.; Tobimatsu, Y.; Jackson, L.; Nakashima, J.; Ralph, J.; Dixon, R.A. Novel seed coat lignins in the Cactaceae: Structure, distribution and implications for the evolution of lignin diversity. *Plant J.* **2013**, *73*, 201–211. [CrossRef]

57. Besseau, S.; Hoffmann, L.; Geoffroy, P.; Lapierre, C.; Pollet, B.; Legrand, M. Flavonoid accumulation in *Arabidopsis* repressed in lignin synthesis affects auxin transport and plant growth. *Plant Cell.* **2007**, *19*, 148–162. [CrossRef]

58. Wang, X.; Elling, A.A.; Li, X.; Li, N.; Peng, Z.; He, G.; Sun, H.; Qi, Y.; Liu, X.S.; Deng, X.W. Genome-wide and organ-specific landscapes of epigenetic modifications and their relationships to mRNA and small RNA transcriptomes in maize. *Plant Cell.* **2009**, *21*, 1053–1069. [CrossRef] [PubMed]

59. Anders, S.; Huber, W. Differential expression analysis for sequence count data. *Genome Biol.* **2010**, *11*, R106. [CrossRef]

60. Fu, W.Q.; Zhao, Z.G.; Ge, X.H.; Ding, L.; Li, Z.Y. Anatomy and transcript profiling of gynoecium development in female sterile *Brassica napus* mediated by one alien chromosome from Orychophragmus violaceus. *BMC Genom.* **2014**, *15*, 61. [CrossRef]

61. Yan, X.; Dong, C.; Yu, J.; Liu, W.; Jiang, C.; Liu, J.; Hu, Q.; Fang, X.; Wei, W. Transcriptome profile analysis of young floral buds of fertile and sterile plants from the self-pollinated offspring of the hybrid between novel restorer line NR1 and Nsa CMS line in *Brassica napus*. *BMC Genom.* **2013**, *14*, 26. [CrossRef] [PubMed]

62. Chalhoub, B.; Denoeud, F.; Liu, S.; Parkin, I.A.; Tang, H.; Wang, X.; Chiquet, J.; Belcram, H.; Tong, C.; Samans, B.; et al. Plant genetics. Early allopolyploid evolution in the post-Neolithic *Brassica napus* oilseed genome. *Science* **2014**, *345*, 950–953. [CrossRef] [PubMed]

63. Slotte, T.; Hazzouri, K.M.; Ågren, J.A.; Koenig, D.; Maumus, F.; Guo, Y.L.; Steige, K.; Platts, A.E.; Escobar, J.S.; Newman, L.K.; et al. The *Capsella rubella* genome and the genomic consequences of rapid mating system evolution. *Nat Genet.* **2013**, *45*, 831–835. [CrossRef]

64. Sun, H.Z.; Wang, D.M.; Wang, B.; Wang, J.K.; Liu, H.Y.; Guan, L.; Liu, J.X. Metabolomics of four biofluids from dairy cows: Potential biomarkers for milk production and quality. *J. Proteome Res.* **2015**, *14*, 1287–1298. [CrossRef] [PubMed]

65. Chen, W.; Gao, Y.; Xie, W.; Gong, L.; Lu, K.; Wang, W.; Li, Y.; Liu, X.; Zhang, H.; Dong, H.; et al. Genome-wide association analyses provide genetic and biochemical insights into natural variation in rice metabolism. *Nat. Genet.* **2014**, *46*, 714–721. [CrossRef] [PubMed]